

International Journal of Quantum Information  
 © World Scientific Publishing Company

## COHERENT CONTROL OF MESOSCOPIC SUPERPOSITIONS IN A DIATOMIC MOLECULE

SURANJANA GHOSH

*Indian Institute of Technology Patna, Patliputra Colony  
 Patna 800013, India  
 sghosh@iitp.ac.in*

Received Day Month Year  
 Accepted Day Month Year

A phase controlled wave packet, recently used in experiment of wave packet interferometry of a diatomic molecule, is investigated to obtain mesoscopic superposition structures, useful in quantum metrology. This analysis provides a new way of obtaining sub-Planck scale structures at smaller time scale of revival dynamics. We study a number of situations for delineating the smallest interference structures and their control by tailoring the relative phase between two subsidiary wave packets. We also find the most appropriate state, so far, for high precision parameter estimation in a system of diatomic molecule.

*Keywords:* Mesoscopic superpositions; Diatomic Molecule; sub-Planck scale structures.

### 1. Introduction

Mesoscopic superposition in different systems has become a benchmark in quantum information processing and quantum metrology<sup>1,2,3,4,5,6,7</sup>. Nonlocal quantum superposition can produce quantum interference structure of dimension below Planck scale, well known as sub-Planck structure (SPS). After the invention of SPS by Zurek<sup>8</sup>, this has attracted an enormous physicists' attention<sup>9,10,11,12,13,14,15,16,17,18,19,20,21</sup>. The fact that these are very sensitive against any external perturbation or decoherence makes them useful for high precision quantum parameter estimation and quantum metrology<sup>11,12,22,23</sup>. Other than systems modeled by harmonic oscillator, obeying Heisenberg-Weyl algebra, SPS was also found in various solvable quantum mechanical potentials, having SU(1,1) and SU(2) symmetries and nonlinear energy spectrums<sup>12,22,23</sup>. Particularly in diatomic molecule (modeled by the Morse potential), SPS was first found in the long time evolution of an appropriately framed coherent state<sup>12</sup>. This application recently brought forward towards the important sensitivity analysis and the effect of decoherence<sup>22</sup>. In the present work, we undertake a new approach, inferred from the experiment where two femtosecond laser pulses whose relative phase was controlled to create a phase-locked vibrational wave packets in iodine molecule<sup>24,25,26</sup>. Recently, in another remarkable work, a spatiotemporal images of quantum inter-

ference on the picometer and femtosecond scale has been reported by using their ultra-precision wave packet interferometry technique<sup>27</sup>. This technique has precise control over the relative phase of the twin optical pulses as well as on the two component subsidiary wave packets. Thus, this method would be capable of monitoring the quantum interference ripples of the phase-locked wave packet. Controlling quantum interference patterns by various means has enormous importance in quantum information science. Here, we show the way of controlling the mesoscopic superposition structures and discuss some results which can't be achieved in the earlier studies using a single localized wave packet dynamics<sup>12,28</sup>. We study this phase locked wave packet, where the relative phase between the two pump pulses plays a crucial role in the system dynamics. This coupled wave packet is capable to capture the signature of the sub-Planck interference structures in Wigner distribution at earlier time as compared to the single coherent state dynamics. In the next section, we elaborate and explain the phase-controlled wave packet, which is followed by the control of the mesoscopic superpositions in spatial domain as well as in phase space. We show how by tuning the relative phase of the wave packets one can actively tailor the quantum interference structures. A systematic numerical analysis yields a compelling evidence to find the most appropriate state, so far in literature, for high precision parameter estimation and quantum metrology in the system of diatomic molecule. We end with some conclusions and future outlook.

## 2. The phase-control wave packet

A wave packet, consisting of two partial wave packets, generated with a pair of femtosecond laser pulses whose relative phase is coherently controlled, can be written as<sup>27</sup>

$$\Phi_{\theta}(\xi, t) = \frac{1}{2} [(1 - e^{i\theta})\Phi_1(\xi, t) + (1 + e^{i\theta})\Phi_2(\xi, t)], \quad (1)$$

where  $\Phi_1(\xi, t)$  and  $\Phi_2(\xi, t)$  are composed of even and odd vibrational levels of a diatomic molecule modeled by Morse potential<sup>12</sup>.  $\xi$  is the variable, related to the internuclear distance, ranging from  $0 < \xi < \infty$ . The parameter  $\theta$  defines the pump-control phase which can be arbitrarily tuned between 0 and  $2\pi$ . As coherent state is most classical in quantum framework and most suitable for studying wave packet dynamics<sup>29</sup>, we use an appropriate SU(2) coherent state, consistent of its dynamical symmetry having finite number of bound states<sup>12</sup>. Individually, the states  $\Phi_1(\xi, t)$  and  $\Phi_2(\xi, t)$  can also be constructed analytically by using a quadratic algebra, which produces superposition of alternate energy levels. This phase locked wave packet allows a nice control over the component  $\Phi_1(\xi, t)$  and  $\Phi_2(\xi, t)$  by tuning the relative optical phases of the laser pulses. The even and odd states result at  $\theta = \pi$  and  $\theta = 0$ , respectively. Otherwise, it is a mixture of both the components involving all energy levels with conserved probability at an arbitrary time  $t$ . The

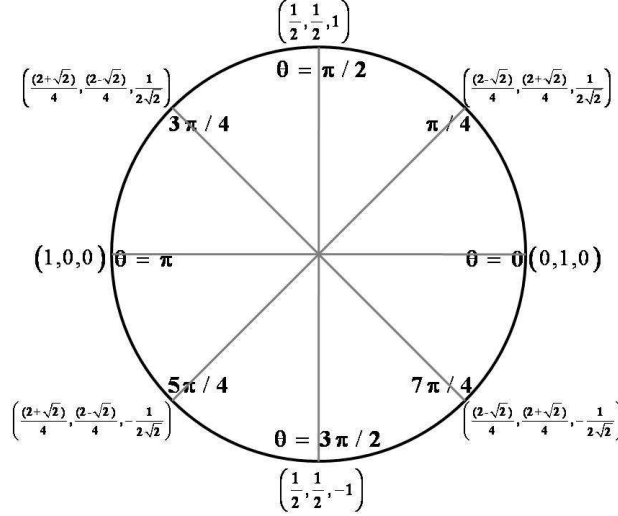


Fig. 1. Phase-circle showing the probability density of the phase controlled wave packet for different  $\theta$ s. Three indices inside the parentheses show the contribution of the even, odd and cross-terms modulo  $|\Phi_1|^2$ ,  $|\Phi_2|^2$  and  $i\sqrt{2}(\Phi_1^*\Phi_2 - \Phi_2^*\Phi_1)$ , respectively.

probability density at any time is given by

$$|\Phi_\theta(\xi, t)|^2 = \frac{1}{4} [(1 - \cos \theta)|\Phi_1(\xi, t)|^2 + (1 + \cos \theta)|\Phi_2(\xi, t)|^2 + i \sin \theta (\Phi_2(\xi, t)\Phi_1^*(\xi, t) - \Phi_1(\xi, t)\Phi_2^*(\xi, t))]. \quad (2)$$

The phase circle in Fig. 1 shows the coefficient of even part, odd part and the cross term of the probability density for different values of  $\theta$  in step of  $\pi/4$ . It is apparent that the cross term for any two states of phase difference ' $\pi$ ' is opposite, which explains the result found in the study of quantum carpets<sup>27</sup>. Now, we define  $\Phi_1(\xi, t)$  and  $\Phi_2(\xi, t)$  as follows

$$\begin{aligned} \Phi_1(\xi, t) &= \sum_{m_1=0}^{m'} d_{m_1} \psi_{m_1}(\xi) \exp^{-iE_{m_1}t} \\ \Phi_2(\xi, t) &= \sum_{m_2=0}^{m'} d_{m_2} \psi_{m_2}(\xi) \exp^{-iE_{m_2}t} \end{aligned} \quad (3)$$

where  $m_1$  and  $m_2$  stand for vibrational quantum numbers corresponding to the even and odd eigenstates  $\psi_{m_1}(\xi)$  and  $\psi_{m_2}(\xi)$ , respectively. Eigenvalues are given by  $E_m = -(D/\lambda^2)(\lambda - m - 1/2)^2$  defining the classical and the revival times,  $T_{\text{cl}} = T_{\text{rev}}/(2\lambda - 1)$  and  $T_{\text{rev}} = 2\pi\lambda^2/D$ , respectively.  $d_m$  yields the weighting factor of the SU(2) coherent state. A detail description and full expressions are given in Ref.<sup>12</sup>. We have used atomic unit ( $\hbar = 1$ ) throughout our study. Here, we consider  $I_2$  molecule and the corresponding parameter values: potential parameter  $\beta = 4.954$ , reduced mass  $\mu = 11.56 \times 10^4$ , equilibrium inter-nuclear distance  $r_0 = 5.03$ , and

4 *Suranjana Ghosh*

dissociation energy  $D = 0.057$ . Coherent state parameter is taken as  $\alpha = 2$ , which includes 24 lower bound states of this molecule.

### 3. Results and Discussions: Control of mesoscopic superpositions and sensitivity analysis

Initially, even and odd probability amplitudes are same and the cross-terms do not exist. Thus, the initial wave packet itself is a combination of two localized components and behaves like a Schrödinger-cat state for arbitrary  $\theta$ . Now it is interesting to see what will happen for longer time evolution. On the other hand, one can observe the changes in the interference structures due to controlled mesoscopic superpositions at particular time. In our further study we mainly concentrate on two typical fractional revival times<sup>30,31,32,33</sup>  $\frac{1}{8}T_{rev}$  and  $\frac{1}{16}T_{rev}$ . The reason behind this are: First, single-wave packet dynamics (SWPD) at  $t = \frac{1}{8}T_{rev}$  results the well studied sub-Planck scale structures originated from a compass-like state (a four way split of a coherent state situated in north-south-east-west directions) in phase space. Hence, it is worth to study what happens by tailoring the phase of the presently considered wave packet. Second, at  $t = \frac{1}{16}T_{rev}$ , SWPD results a eight-fold wave packet or a combination of two imprinted compass-like states. Thus, this state would be more interesting to investigate in the present scenario. Moreover, the coherent control admits both lower and higher order mesoscopic superpositions at a particular time in contrast to the SWPD. So we expect some interesting features in both the cases, which are the consequences of cross-diagonal superpositions. It is difficult to resolve further higher order superpositions at higher order fractional revival times due to limited phase space support and asymmetry of the potential.

#### 3.1. Control of Spatial Ripples

We start with the control of spatial ripples, through the exploration of quantum carpets tailored by  $\theta$  at two specific times mentioned above (see Fig. 2). The quantum carpet is characterized by the maxima and minima of probability stretching out in a space-phase representation. At  $t = \frac{1}{8}T_{rev}$ , Fig. 2(a) shows how the controlled relative phase designs the present carpet. For  $\theta = 0$ , probability distribution resembles the initial phase-locked wave packet, which is a cat-state. However, the spatial interference ripples begin to rise and acquire maximum value at  $\theta = \pi$ , where the component wave packets fully overlap in coordinate space. The ripples vanishes again at  $\theta = 2\pi$ , resulting a spatially separated cat state. The second case,  $t = \frac{1}{16}T_{rev}$ , as shown in Figure 2(b), is bit nontrivial. Spatial ripples are present

Table 1. Variation of the amplitude of interference maxima  $A_m$  with  $\theta$  at  $t = \frac{1}{8}T_{rev}$ .  $A_m$  has dimension  $[L]^{-1}$  and is in atomic unit.

$\theta$	0	$\pi/8$	$\pi/4$	$3\pi/8$	$\pi/2$	$5\pi/8$	$3\pi/4$	$7\pi/8$	$\pi$
$A_m$	0.0	0.305	1.14	2.39	3.85	5.31	6.54	7.35	7.63

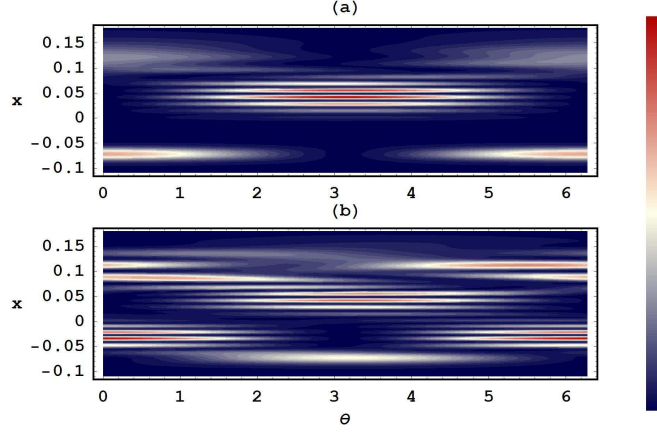


Fig. 2. (Color online) Quantum carpet shows the phase-control of the probability density at one-eighth (a) and one-sixteenth (b) of revival times, respectively. Here  $x = r/r_0 - 1$ , is the dimensionless variable,  $r$  and  $r_0$  both are in the a.u, whereas  $\theta$  varies between  $0 \leq \theta \leq 2\pi$  radians.

both at initial and final stages. In addition, we get some extra ripples in between, interpretation of which is not obvious from this plot. It captures mostly the superposition structures instead of individual counterparts. For further clarification, we will recall it while explaining the phase space distribution. In the first case, we have numerically estimated the amplitude of the highest interference ripples ( $A_m$ ) at  $\frac{1}{8}T_{rev}$  (Table. 1). It reveals the influence of  $\theta$  on  $A_m$ , where  $A_m$  starts from 0 at  $\theta = 0$  and gradually regains maximum value for  $\theta = \pi$ . For the rest of the interval,  $\pi$  to  $2\pi$ , it is a mirror image of the first half. It is worthy to note that for a fixed evolution time, one is able to control quantum ripples which signifies the signature of quantum character.

### 3.2. Control of Phase-space structures

The mesoscopic superposition structures are the result of nonlocal superpositions of quantum states, best displayed in the phase space Wigner representation:

$$W(x, p, t) = \frac{r_0}{\pi} \int_{-\infty}^{+\infty} \Phi^*(x - x', t) \Phi(x + x', t) e^{-2ipx'} dx', \quad (4)$$

where  $x$  coordinate is related with  $\xi$  as  $\xi = 2\lambda e^{-\beta x}$  and  $x = r/r_0 - 1$ . Negative regions in the oscillatory structures of this function indicate non-classicality. Sub-Planck scale structures usually appear as alternate small ‘tiles’ of maxima and minima. The phase space area of these ‘tiles’ are much less than  $\hbar$  (1 in a.u.). It is inversely proportional to the effective phase-space area globally occupied by the state, which can be significantly larger than  $\hbar$ . These structures are very sensitive to environmental decoherence<sup>8,10,22</sup> and have important applications in Heisenberg-limited measurements and quantum parameter estimation<sup>11,13,23</sup>. We have shown

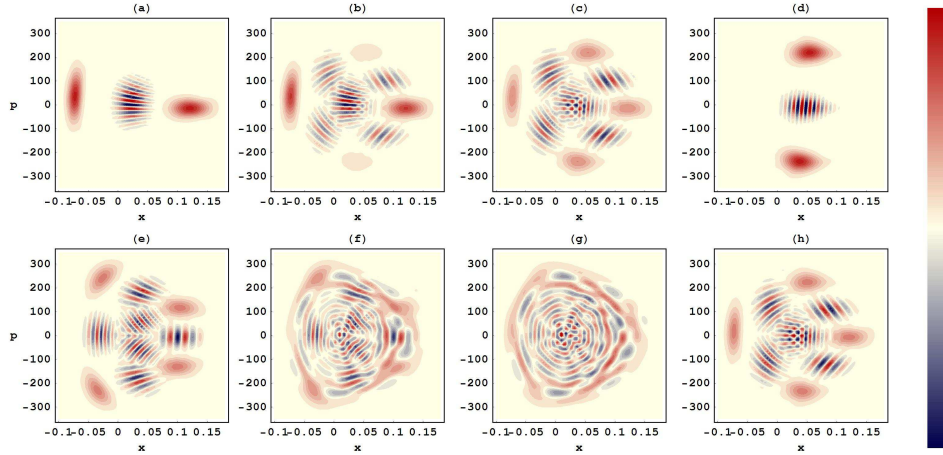
6 *Suranjana Ghosh*

Fig. 3. (Color online) Wigner distribution of phase locked wave packets at  $t = \frac{1}{8}T_{rev}$  (a)-(d) and  $t = \frac{1}{16}T_{rev}$  (e)-(h) for different  $\theta$  (0,  $\pi/4$ ,  $\pi/2$ , and  $\pi$ ). Here,  $x$  and  $p$  are the dimensionless position and momentum, where  $x = r/r_0 - 1$  and  $p$  is the corresponding scaled variable.

schematically the Wigner functions at  $t = \frac{1}{8}T_{rev}$  (Fig. 3 (a)-(d)) and  $t = \frac{1}{16}T_{rev}$  (Fig. 3 (e)-(h)) for different  $\theta$ s. We show how these structures can be controlled by tailoring the phase. In Fig. 3(a), null phase signifies a cat state thus the initial phase locked wave packet is reviving at  $\frac{1}{8}T_{rev}$ . This is significantly different from SWPD. The exact contribution of even and odd parts of probability density can be seen from the phase circle (see Fig. 1). Another crucial factor is how even and odd states behave at some particular time. At certain time, the diversity in mesoscopic superposition structures arise due to the competing two components associated with even and odd parts. In Fig. 3, first row manifests compass-like state for all  $\theta$  except  $\theta = 0$  and  $\pi$ . In the last case (Fig. 3(d)), this is again a cat state localized in momentum regime. Thus, one can monitor the interference ripples, either in position or in momentum space. With increasing value of  $\theta$ , even parts starts to contribute appreciably (see Fig. 3(b)). At  $\theta = \pi/2$ , we obtain well define sub-Planck tiles originated from compass-like state where the even and odd parts contributed commensurately. The structures at  $t = \frac{1}{16}T_{rev}$  (see second row of Fig. 3) are more interesting. In Fig. 3(e) and 3(h), the exact control over  $\theta$  gives rise to compass-like states at earlier time than SWPD in which it usually takes place at  $\frac{1}{8}T_{rev}$ . Moreover, 3(e) reveals a different kind of compass state (not a ‘north-south-east-west’-kind like 3(h) and 3(c)), may have extra importance as we are dealing with the asymmetric potential. Figure 3(f) and 3(g) both are eight-fold mesoscopic superposition or overlap of two compass-like states. A better explanation of the quantum carpet as shown in Fig. 2(b) can be found from the phase space description as displayed in Fig. 3(e)-(h). We need to perform a quantitative analysis for

revealing the advantages of this method than the earlier one<sup>12</sup>.

### 3.3. Quantitative study

The smallest structures in the interference regime appear as alternate positive and negative tiles of sub-Planck dimension. The phase-space area occupied by the tiles ‘ $a$ ’ scales as  $\sim \hbar^2/A$  ( $\sim 1/A$  in atomic units), where  $A$  is the classical action of the state.  $A$  is approximately given by the product of the effective support of its

Table 2. Tailoring the dimension (in atomic unit) of sensitive mesoscopic superposition (sub-Planck) structures with  $\theta$  at two typical times.

$\theta$	0	$\pi/8$	$\pi/4$	$3\pi/8$	$\pi/2$	$5\pi/8$	$3\pi/4$	$7\pi/8$	$\pi$
$\frac{1}{8}T_{rev}$	0.185	0.148	0.108	0.089	0.083	0.089	0.109	0.157	0.210
$\frac{1}{16}T_{rev}$	0.0766	0.0769	0.0776	0.0786	0.0800	0.0814	0.0827	0.0835	0.0837

state in position and momentum:  $A \sim \Delta x \times \Delta p$ , where  $\Delta x = \sqrt{\langle x^2 \rangle - \langle x \rangle^2}$  and  $\Delta p = \sqrt{\langle p^2 \rangle - \langle p \rangle^2}$ . In Table 2, we have numerically evaluated the uncertainty products and the area of the smallest tiles both at  $\frac{1}{8}T_{rev}$  (second row) and  $\frac{1}{16}T_{rev}$  (third row), respectively. The most important property of these sub-Planck tiles is the fact that the corresponding quantum state is extremely sensitive to external perturbation. This sensitivity is also represented by the well-known formula<sup>2</sup>:

$$|\langle \Phi | \Phi' \rangle|^2 = \int \int W(x, p) W'(x, p) dx dp, \quad (5)$$

where  $W$ ,  $W'$  are the Wigner functions of the unperturbed  $|\Phi\rangle$  and the perturbed  $|\Phi'\rangle$  quantum states respectively. The perturbed and unperturbed states become distinguishable when a single tile (maxima or minima) of the interference structure is displaced due to a small external perturbation and its maximum coincides with a minimum of the undisplaced state. Thus, one has destructive interference and the two states become approximately orthogonal and distinguishable. Therefore these structures determine the limit of sensitivity of the system. We observe few robust behaviors: first, if we compare column-wise, area of the tiles in the third row is always smaller than that of the second row for all  $\theta$ . Hence, the structures in Fig. 3 (e)-(h) are more sensitive than in Fig. 3 (a)-(d); second, the tiles in the three cases, *i.e.*, in Fig. 3(c), Fig. 3(e), and Fig. 3(h), are all originated from compass-like states. Upon comparing the area, we find that the structures of the new compass-like state in Fig. 3(e) are smallest and most sensitive among these three cases. In fact, this provides the smallest structures among all the other mesoscopic superpositions structures in phase space hence improving the sensitivity limit in the literature.

### 3.4. Conclusions

We have shown a way to control the sensitive mesoscopic superposition structures in a diatomic molecule. The wave packet can be observed at a particular time and then

relative phase between the two pulses can be controlled coherently. The sub-Planck interference structures play very important role in high precision parameter estimation and quantum metrology. Even at a definite time, we show how one can obtain either higher or lower order superpositions by tailoring the phase. It is worth mentioning that one of the difficulties to realize these structures in experiments is the default system-environment interaction, which results the structures decay before reaching to that desired time. Although, very recently there are few experiments demonstrating decoherence in a controlled way, this issue still remains a big hurdle in quantum information science. Hence, physicists always keep their eyes to find various methods to create SPS in quantum systems. Primarily, we show the way to create and control these structures in diatomic molecule. In addition, it has also found several extra advantages over the earlier one. First of all, our method is capable of obtaining the SPS at smaller evolving time with respect to earlier methods and this minimizes the difficulty to observe these structures in presence of decoherence. Secondly, we indicate the most sensitive (smallest) structures, appeared in a new type of compass state in diatomic molecule. We intend to study the decoherence of this state in future, and also look over the application in quantum computation.

#### 4. Acknowledgments

The author acknowledges the financial support provided by the Department of Science and Technology, Govt. of India (Fast Track project No. *SR/FTP/PS* – 062/2010).

#### References

1. W. Schleich and J. A. Wheeler, *Nature* **326** (1987) 574.
2. W. Schleich and J. A. Wheeler, *J. Opt. Soc. Am. B* **4** (1987) 1715.
3. W. Schleich, D. F. Walls, and J. A. Wheeler, *Phys. Rev. A* **38** (1988) 1177;
4. W. P. Schleich, *Quantum Optics in Phase Space* (Wiley-VCH, Berlin, 2001) and references therein.
5. L. Davidovich, M. Brune, J. M. Raimond, and S. Haroche, *Phys. Rev. A* **53** (1996) 1295.
6. J. M. Raimond, M. Brune, and S. Haroche, *Phys. Rev. Lett.* **79** (1997) 1964.
7. A. Auffeves et al., *Phys. Rev. Lett.* **91** (2003) 230405.
8. W. H. Zurek, *Nature* **412** (2001) 712.
9. Ph. Jacquod, I. Adagideli, and C. W. J. Beenakker, *Phys. Rev. Lett.* **89** (2002) 154103.
10. P. K. Pathak and G. S. Agarwal, *Phys. Rev. A* **71**(2005) 043823.
11. F. Toscano, D. A. R. Dalvit, L. Davidovich, and W. H. Zurek, *Phys. Rev. A* **73** (2006) 023803.
12. S. Ghosh, A. Chiruvelli, J. Banerji, and P. K. Panigrahi, *Phys. Rev. A* **73** (2006) 013411.
13. D. A. R. Dalvit, R. L. de M. Filho, and F. Toscano, *New Journal of Physics* **8** (2006) 276.
14. L. Praxmeyer, P. Wasylczyk, C. Radzewicz, and K. Wódkiewicz, *Phys. Rev. Lett.* **98** (2007) 063901.



15. J. Banerji, *Contemp. Phys.* **48** (2007) 157.
16. J. R. Bhatt, P. K. Panigrahi, and M. Vyas, *Phys. Rev. A* **78** (2008) 034101.
17. M. Stobinska, G. J. Milburn, and K. Wódkiewicz, *Phys. Rev. A* **78** (2008) 013810.
18. A. J. Scott and S. M. Caves, *Annals of Physics* **323** (2008) 2685.
19. D. R. Austin, T. Witting, A. S. Wyatt, and I. A. Walmsley, *Opt. Commun.* **283** (2010) 855.
20. E. I. Jafarov, J. Van der Jeugt, *Physics Letters A* **374** (2010) 3400.
21. S. Ghosh and I. Marzoli, *Int. J. Quantum Information* **9** (2011) 1519.
22. S. Ghosh, U. Roy, C. Genes, and D. Vitali, *Phys. Rev. A* **79** (2009) 052104.
23. U. Roy, S. Ghosh, P. K. Panigrahi, and D. Vitali, *Phys. Rev. A* **80** (2009) 052115.
24. N. F. Scherer, R. J. Carlson, M., Du M. Alexander, J. Ruggiero, V. Romero-Rochin, J. A. Cina, G. R. Fleming, and S. A. Rice, *J. Chem. Phys.* **95** (1991) 1487.
25. N. F. Scherer, A. Matro, L. D. Du M. Ziegler, R. J. Carlson, J. A. Cina, and G. R. Fleming, *J. Chem. Phys.* **96** (1992) 4180.
26. H. Katsuki, H. Chiba, C. Meier, B. Girard, and K. Ohmori, *Phys. Chem. Chem. Phys.* **12** (2010) 5189.
27. H. Katsuki, H. Chiba, C. Meier, B. Girard, and K. Ohmori, *Phys. Rev. Lett.* **102** (2009) 103602.
28. H. Katsuki, H. Chiba, B. Girard, C. Meier, and K. Ohmori, *Science* **311** (2006) 17.
29. A. M. Perelomov, *Generalized Coherent States and Their Applications* (Springer, Berlin, 1986).
30. J. Parker and C. R. Stroud, *Phys. Rev. Lett.* **56** (1986) 716.
31. G. Alber G, H. Ritsch, and P. Zoller, *Phys. Rev. A* **34** (1986) 1058.
32. I. Sh Averbukh and N. F. Perelman, *Phys. Lett. A* **139** (1989) 449.
33. R. W. Robinett, *Phys. Rep.* **392** (2004) 1 and references therein.